Eur. Phys. J. D **19**, 315–325 (2002)
DOI: 10.1140/epjd/e20020090

THE EUROPEAN PHYSICAL JOURNAL D
EDP Sciences

Merged beam study of the associative ionisation (C^+, N^+ and O^+) + O^-

T. Nzeyimana[1], E.A. Naji[1], X. Urbain[1], and A. Le Padellec[2,a]

[1] Unité FYAM, Département de Physique, Université Catholique de Louvain, chemin du cyclotron 2, 1348 Louvain-La-Neuve, Belgium
[2] LCAR[b], Université Paul Sabatier-Toulouse III, 118 route de Narbonne, bâtiment IIIR1b4, 31062 Toulouse Cedex 4, France

Received 10 December 2001 and Received in final form 12 March 2002

Abstract. Total cross-sections have been measured for the associative ionisation of $C^+ + O^-$, $N^+ + O^-$ and $O^+ + O^-$ by means of a merged-beam set-up operating with keV beams. These original measurements might be relevant to the understanding of some astrophysical objects or laboratory-made plasmas (flames and etching plasmas). The magnitude of these cross-sections is particularly large whatever the associating system, as these are in the range of 1×10^{-14} cm^2 at thermal energies. Their behaviour as a function of energy significantly differs from one system to another, and is characterised by the Wigner law at low energy, and a rapid fall-off at higher energy due to competition with non-associative ionisation processes.

PACS. 82.30.Nr Association, addition, insertion, cluster formation – 31.10.+z Theory of electronic structure, electronic transitions, and chemical binding – 95.30.Ft Molecular and chemical processes and interactions

1 Introduction

Among the possible reaction mechanisms leading to the formation of diatomics in binary collisions, associative ionisation is the fastest one, as autoionisation may occur on the same timescale as the collision, while photon emission is slower by several orders of magnitude. The latter process, *i.e.* radiative association, is often considered as dominant in space, since excited atomic reactants are needed for associative ionisation to proceed. An exothermic AI channel exists, that involves negative and positive ions. However, negative ions are easily destroyed by radiation and charge exchange, reducing the possible contribution of the process to the global molecular synthesis, and explaining why the reactions between ions have been overlooked in astrophysical considerations.

Carbon monoxide was detected in emission in the spectrum of supernova 1987A, and probably also its ion, CO^+ (see Ref. [1]). Dalgarno *et al.* [2] listed possible mechanisms that would lead to these species, and among them, they focused on the radiative association (RA) processes:

$$C + O \rightarrow CO + h\nu, \tag{1}$$

$$C^+ + O \rightarrow CO^+ + h\nu. \tag{2}$$

At room temperature, they calculated RA rate coefficients of 0.21 and 2.5 in 1×10^{-18} cm^3 s^{-1} units, for approach along the $CO(A^1\Pi)$ and $CO^+(A^2\Pi)$ states, respectively. These are indeed very low rates. Moreover, they did not consider as an alternative to the production of the ion, the associative ionisation (AI) process:

$$C + O \rightarrow CO^+ + e \tag{3}$$

most probably due to the endothermicity of this reaction for the four lowest neutral pairs C + O (2.92 eV for the ground state reactants). Nevertheless, the upper pairs give rise to an exothermic process (3), as in the case of AI between charged reactants

$$C^+ + O^- \rightarrow CO^+ + e \tag{4}$$

which is the subject of the present paper. Similarly, the latter reaction was not listed as a possible source of carbon monoxide cations in reference [2]. This is indeed a little bit surprising since in a review article published two years afterwards, Dalgarno [3] included in his reaction scheme the fragile O^- anion for the mantle chemistry of the supernova and considered its immediate destruction through the associative detachment process:

$$C + O^- \rightarrow CO + e. \tag{5}$$

This would imply that process (5) is held for even more efficient in terms of the O^- removal than the AI process,

[a] e-mail: arnaud.lepadellec@irsamc.ups-tlse.fr
[b] UMR 5589

but the very large total cross-sections to be presented below tend to contradict that assumption.

The $N + O$ radiative association process and its reverse, the photodissociation, was the subject of an experimental investigation by Mandelman *et al.* [4]. Their main result concerns the total RA rate coefficient for which they found a value of 15×10^{-18} cm^3 s^{-1}, without indication of the temperature this would refer to. There is another exit channel that results from the $N + O$ collision and gives rise to the associative ionisation process. Particular emphasis was put on:

$$N(^4S, ^2D) + O(^3P) \rightarrow NO^+(\Sigma^+) + e \qquad (6)$$

both theoretically, by Nielsen and Dahler [5] and experimentally for $N(^2D)$, by Ringer and Gentry [6], in a merged molecular beam. Cross-sections as large as 0.6×10^{-16} cm^2 were found at the maximum of the experimental curve. Moreover, Bertrand and van Tiggelen [7], and Bredo *et al.* [8] acknowledged the process:

$$N(^2D, ^2P) + O(^3P) \rightarrow NO^+ + e \qquad (7)$$

to be the primary source of the nitrogen oxide cations in ammonia and hydrogen-oxygen-nitrogen flames. The contribution of the AI process that arises from the charged reactants $N^+ + O^-$, and for which we will present below the total cross-sections, is not mentioned by these authors, as collisional detachment of negative ions is assumed to prevail in hot environments.

The radiative association and inverse predissociation of oxygen atoms, were the subject of a theoretical work by Babb and Dalgarno [9] using quantum-mechanical methods. They found at temperatures below 1 000 K that the RA process occurs by approach along the $1^3\Pi_u$ state of O_2 whereas above the same temperature, the inverse predissociation through the $B^3\Sigma_u^-$ is the dominant mechanism. Capitelli and Ficocelli [10] reported about collision integrals of oxygen atoms in different electronic states. More particularly, they provide us with informations for the interaction $O(^3P) + O(^3P)$, considering both repulsive and bound states of O_2. To the best of our knowledge, there is no available information in the literature about the associative ionisation process leading to the O_2^+ ion, neither originating from $O + O$, nor from $O^+ + O^-$. We will present below the total cross-sections for the latter reaction.

The paper is organised as follows. The next section will present the experimental set-up and changes with respect to the previous studies. Then, the experimental procedure will be described and the complications that arise from the degree of electronic excitation of the target cations as well as to the finite energy resolution of the apparatus are highlighted. This is followed by the presentation and discussion of our experimental results and this section is divided into three parts, corresponding to the $C^+ + O^-$, $N^+ + O^-$ and $O^+ + O^-$ systems, respectively. A conclusion is finally given.

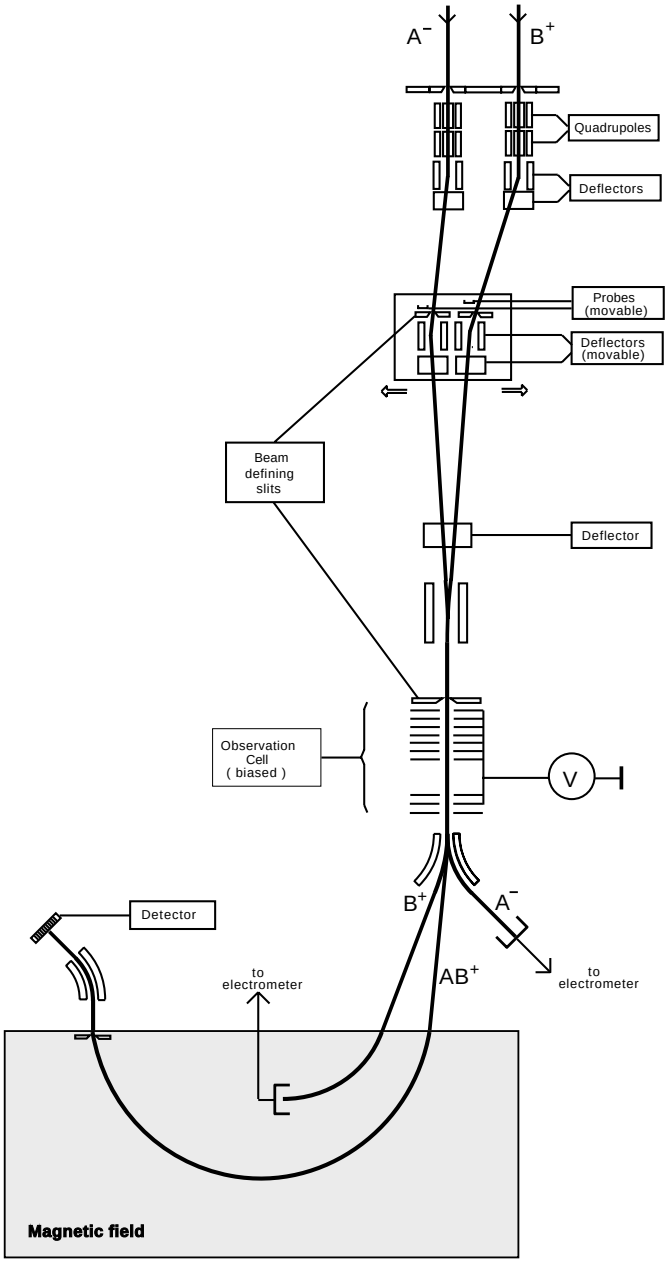

Fig. 1. Sketch of the merged beam apparatus.

2 Experimental set-up and changes with respect to previous studies

Although the description of the experimental set-up can be found in recent published works [11–13], some modifications were recently achieved that we shall report on, together with the main features of the technique. The whole machine can be divided into four sections pumped in ultra high vacuum as shown in Figure 1. The first one includes the ion sources, the acceleration, the mass selectors as well as the beam optics. The second one is the place where the two ionic beams are merged and animated, whereas the third one corresponds to the 6.8 ± 0.2 cm long interaction region (see below the discussion). The last one

contains the magnetic analyser where the intensities of the primary beams are recorded and the reaction products detected (the molecular cation for the associative ionisation process). Since the second and third regions have not been modified, we will focus our description on the two other parts.

The main changes in the first region concern the cationic primary beam (here C^+, N^+ and O^+). The previously used Wien filter was removed and the mass selection is now achieved upstream, just after the electron cyclotron resonance (ECR) ion source outlet, by means of a 30° magnetic sector. Moreover, the cylindrical deflector and quadrupole lenses formerly placed further downstream were also removed and replaced by a spherical deflector and an electrostatic lens, respectively. The only change that concerns the anionic primary beam (here O^-) deals with the use of a prismatic lens placed just downstream to the cylindrical deflector. The goal of all of these changes was the improvement of the quality and intensity of the beams. There were also some changes in the fourth region where the detection of the reactants and products takes place. The Faraday cup to monitor the primary anionic beam was redesigned. More importantly, a cylindrical deflector was added at the outlet of the magnetic analyser before the channeltron detector that records the molecular cations. This allowed a drastic reduction of the noise hitting the detector.

3 Experimental procedure

The number of reactions N that occur within a certain time T in a merged beam set-up, is connected to the absolute cross-section σ by the following expression:

$$N(T) = \sigma \frac{v_\mathrm{r}}{q_1 q_2 v_1 v_2} \int_0^T \mathrm{d}t \int_L \mathrm{d}z \times \int_{-\infty}^{+\infty} \int_{-\infty}^{+\infty} j_1(x,y,z,t) j_2(x,y,z,t) \mathrm{d}x\,\mathrm{d}y \quad (8)$$

where v_r, v_1, v_2, q_1, q_2, j_1, j_2 depict the relative velocity, the laboratory velocities, the charges and the current densities of the two beams, respectively, and L is the interaction length.

Equation (8) may be rewritten to separate the beam intensities from their geometrical distribution:

$$N(T) = \sigma \frac{v_\mathrm{r}}{q_1 q_2 v_1 v_2} F \int_0^T I_1(t) I_2(t)\,\mathrm{d}t \quad (9)$$

where I_1 and I_2 represent the currents of the target ions, and the parameter F is the so-called form factor that accounts for the degree of overlap of the two interacting beams and is assumed to be time independent in the expression given above. Its mathematical formulation is:

$$F = \frac{\int_L \mathrm{d}z \int_{-\infty}^{+\infty} \int_{-\infty}^{+\infty} j_1(x,y,z) j_2(x,y,z) \mathrm{d}x\,\mathrm{d}y}{\int_{-\infty}^{+\infty} \int_{-\infty}^{+\infty} j_1(x,y,z) \mathrm{d}x\,\mathrm{d}y \int_{-\infty}^{+\infty} \int_{-\infty}^{+\infty} j_2(x,y,z) \mathrm{d}x\,\mathrm{d}y}. \quad (10)$$

The form factor is a critical parameter in an absolute cross-section determination but it is also non-trivial to evaluate, since it involves the measurement of the density profiles of the two interacting beams. However, there is a method that allows one to overcome this difficult measurement. Indeed, if the two beams exhibit a sharply characterised section, that means uniform densities, but also fully overlap over a known region L, the form factor is simply expressed by:

$$F = \frac{L}{S_>} \quad (11)$$

where $S_>$ denotes the section of the largest beam. In practice, the conditions to apply this simplified expression are fulfilled by strongly diaphragming the two beams just before they interact, namely by only making use of the cores of the two reactant beams. This is of course at the expense of the beam intensities. From the latter formula, it is also clear that the interaction length L shall be defined cautiously. This is achieved by applying a certain observation voltage V to the interaction region. As a result, the molecular cations formed in this region experience an increase of their kinetic energy by an amount +eV and become completely distinguishable, after magnetic analysis, from other molecular cations produced anywhere else. The interaction length is therefore equal to that of the region where the electric potential is equal to V and the 3% uncertainty, quoted above, is determined both by the (known) energy resolution of the magnetic analyser (connected to the energy dispersion of the two interacting beams) and the inhomogeneity of the potential at the entrance and exit regions of the interaction region where gradients take place.

The kinematics of the merged beam experiment gives the centre-of-mass energy E_cm:

$$E_\mathrm{cm} = \mu \left[\sqrt{\frac{q_2(A_2 - V)}{m_2}} - \sqrt{\frac{q_1(A_1 - V)}{m_1}} \right]^2 \quad (12)$$

with μ, A_1, A_2, m_1 and m_2, the reduced mass, accelerating voltages and masses, respectively. Thus, a fine adjustment of the centre-of-mass energy can be achieved by changing the observation voltage and more specifically, low centre-of-mass energy cross-sections are measurable down to 10 meV, provided that a critical analysis of the energy resolution is performed (see below). In the present measurements, the acceleration voltages for the C^+, N^+, O^+ and O^- ionic beams were 7, 7, 6 and −7 kV, respectively and therefore, the theoretical observation voltages (for zero centre-of-mass energy) were 1 000, 467 and −500 V for the $C^+ + O^-$, $N^+ + O^-$ and $O^+ + O^-$ systems, respectively. The beam intensities were 58, 80 and 30 nA for C^+, N^+ and O^+, respectively, whereas it ranged between 16.5 and 30 nA for O^-, depending upon the set of measurements. The detection efficiency for the collection of the molecular ions has been measured to be 98%, by coincidence measurements of collision-induced dissociation of diatomics [14].

The number of counts $N(T)$ of molecular cations produced by the associative ionisation process is measured with the channeltron detector located at the end of the analysing system. Although the background contribution was seriously reduced with the adjunction of a cylindrical deflector, it had to be evaluated for the same acquisition time T and subtracted from the apparent signal. This was achieved by chopping the anionic beam and recording the signal with anions ON and OFF, provided that this beam did not give any background contribution by itself, which was verified by stopping the cationic beam.

Before we present our data that deal with the associative ionisation process in $C^+ + O^-$, $N^+ + O^-$ and $O^+ + O^-$ collisions, we would like to emphasise possible complications in their analysis, due to the experimental configuration. In the next paragraph, we will treat both questions related to the possible degree of electronic excitation of the cationic targets and to the energy resolution in the center-of-mass frame.

4 Degree of electronic excitation of the target ions and energy resolution

The cationic beams were produced within the ECR ion source, located about 2.6 m upstream from the interaction region. The C^+ cations on one hand, the N^+ and O^+ cations on the other hand, were produced from electron impact dissociation on pure carbon monoxide CO and nitrous oxide N_2O, respectively. The anionic beam O^- was extracted off-axis from a duoplasmatron ion source filled with pure N_2O. If the electronic excitation of the target beam O^- is obvious, since only the ground state $2p^5\ ^2P_{3/2}$ is stable, the answer to the same question for the cationic counterparts is far from being as simple, and the piece of elements that we shall develop are twofold. Are the cations produced in excited states using the gases mentioned above? If so, do they have time to relax during the residence time within the source and the time of flight prior to reach the interaction region? It should be pointed out that we did not have to face such problems in earlier studies like the one concerning $He^+ + H^-(D^-)$ [12], because the first excited ^2P state of He^+ lies far above the ^2S ground state, *i.e.* 40.8 eV.

For C^+ and below 10 eV, in addition to the ^2P ground state, there are two excited states, the ^4P and ^2D lying at 5.33 and 9.29 eV, respectively [15]. For N^+ and below 6 eV, there are three states above the ^3P ground state, the ^1D, ^1S and ^5S, at 1.90, 4.05 and 5.85 eV, respectively [15]. For O^+ and below 6 eV, there are two states above the ^4S ground state, namely the ^2D and ^2P at 3.32 and 5.02 eV, respectively [15]. An additional contamination might arise from the presence in the beams of doubly charged molecular cations that have the same charge-to-mass ratio as singly charged atomic cations. Nevertheless, the large threshold energies needed for their productions suggest that they were unlikely to be present in significant proportions within the ECR ion source.

4.1 Production of C^+ cations from CO

There are few data in the literature on that subject, and there are even fewer that treat the electronic excitation of the C^+ cation. One has to consider an early study by Ajello [16] who reports the so-called carbon lines at the end of his paper. He stressed the fact that the strongest atomic feature in his vacuum ultraviolet spectrum was the C^+ multiplet at 1 335 Å, and assigned this to the $C^+(^2D \rightarrow {}^2P)$ transition. This is an experimental evidence that we might have also populated at least the $C^+(^2D)$ and therefore the less excited $C^+(^4P)$ in our C^+ beam.

4.2 Production of N^+ and O^+ cations from N_2O

Two works are of interest for us, one dealing with the photoionisation mechanisms on N_2O and subsequent ion dissociation by Berkowitz *et al.* [17], the other one dealing with the oscillator strength measurement for the ionic photofragmentation, by Hitchcock *et al.* [18]. At low photon energy, Berkowitz *et al.*'s explanation to the formation of O^+ is the autoionisation of Rydberg states converging to the $\tilde{A}\,^2\Sigma^+$ ionic core, that presumably further populate the $^4A''$ ionic surface in the bent Cs geometry. This latter surface lies between $\tilde{X}^2\Pi$ the and $\tilde{A}\,^2\Sigma^+$ linear ionic states, and correlates with the repulsive $^4\Sigma^-$ in the asymptotic linear region. Nevertheless, only the higher portions of the $^4A''$ surface (higher vibrational levels) are energetically capable of yielding $O^+(^4S) + N_2(X^1\Sigma_g^+)$. Concerning the N^+ production, the same authors mention the possible role of the $\tilde{C}^2\Sigma^+$, but also point out the collision induced dissociation. The work by Hitchcock *et al.* [18] gives support to the last point, since they also mention that the O^+ and N^+ fractions were significantly pressure dependent. They suggest a "characteristic ionic fragmentation process" that would involve a total breakup of N_2O^+ that results from the autoionisation of associated Rydberg states, and speculate that the atomic constituents might be released with a random distribution of the positive charges. This does not exclude electronically excited N^+ and O^+ cations to be produced.

Moreover, the presence of electronically excited cations N^+ and O^+ was explicitly highlighted by Hamdan and Brenton [19] on one hand, and by Reid [20] on the other hand, who show that about 45% of the O^+ cations produced by electron impact of O_2 were in the ^2P and ^2D metastable states over a broad electron energy range. Evidence of similar metastable contamination was also demonstrated by Harrison *et al.* [21] in their N^+ ion beam, in particular with the ^1D and ^1S states.

4.3 Decay of excited cations

One has to evaluate the residence time of the cations within the ECR source, add their time of flight to the interaction region, and compare the numbers with the different possible transition lifetimes of the cations. The residence time can be evaluated from Blakley *et al.* [22]

(see also Sheehan *et al.* [23]). For a six centimeters inner diameter cylindrical ion source and for a typical pressure of 9×10^{-5} mbar, these residence times are 1.4, 2.0 and 2.1 μs, for C^+, N^+ and O^+, respectively. The corresponding times of flight are 8.4, 8.7 and 9.3 μs, respectively.

For the C^+ cations, the radiative lifetimes corresponding to the $^2D \rightarrow {}^2P$ and $^4P \rightarrow {}^2P$ transitions, are 3.5 ns and at least 6.7 ms, respectively. This means that if ever produced (and there is evidence it was), the ^2D state might have had time to decay entirely, and therefore our C^+ beam might have been comprised of a mixture C^+ (^2P and ^4P) of unknown proportion. For the N^+ cations, the radiative lifetimes corresponding to the $^3D \rightarrow {}^3P$, $^5S \rightarrow {}^3P$, $^1S \rightarrow {}^1D$ and $^1D \rightarrow {}^3P$ transitions, are 2.6 ns and at least 5.5 ms, 855 ms and 275 s, respectively. It is clear that, if ever produced, the ^5S, ^1S, ^1D and ^3P states of N^+ were populated. For the O^+ cations, the radiative lifetimes corresponding to the $^2P \rightarrow {}^4S$ and $^2D \rightarrow {}^4S$ transitions, are at least 19 and 6 290 s, respectively. The lifetime value for the fully allowed $^2P \rightarrow {}^2D$ transition is in the nanosecond scale. Therefore, if ever produced, the ^2D and ^4S states of O^+ were populated in the interaction region. It shall be stressed that we did not include possible collisional quenching within the ECR source because of the lack of data on the subject, but it is unlikely, since the pressure in the source was rather low, as mentioned above.

4.4 Collision energy resolution

This is a very important matter as already stressed above, especially for the low centre-of-mass energy data that we will present next. We treated this issue in the following way. The form factor and collision velocity distributions are obtained by numerical simulation of the particle distribution limited by the set of defining apertures (1.5 mm in diameter), present along both beam trajectories. The interaction volume is discretised, and all possible pairs of trajectories emerging from discrete surface elements of the first defining aperture are considered, provided they are transmitted by the second defining aperture located at the entrance of the biased interaction region. The angle formed by the velocity vectors is computed, and the corresponding histogram built. Finally, the collision energy distribution $F(E_{\rm cm})$ is obtained by folding this angular distribution $f(\theta)$ with the Gaussian energy spread of both beams, $g(E_i)$ (our model assumes 5 eV FWHM of energy dispersion for both ionic beams), using the equation relating the collision energy to the particle velocity vectors:

$$F(E_{\rm cm}) = \iiint g(E_1)g(E_2)f(\theta) \times \delta\left(E_{\rm cm} - \mu\left[\frac{E_1}{m_1} + \frac{E_2}{m_2} - 2\sqrt{\frac{E_1E_2}{m_1m_2}}\cos\theta\right]\right) {\rm d}E_1{\rm d}E_2{\rm d}\theta. \quad (13)$$

The apparent cross-section is obtained by dividing the reaction rate by the velocity detuning $v_{\rm d}$ (defined for rigorously parallel and monoenergetic beams):

$$\sigma_{\rm app} = \int \sigma(E_{\rm cm})\frac{\nu_{\rm cm}}{\nu_{\rm d}}F(E_{\rm cm}){\rm d}E_{\rm cm}. \quad (14)$$

In the case of pure Coulomb interaction, the cross-section behaves like $E_{\rm cm}^{-1}$ in the low energy limit, and the apparent cross-section is then:

$$\sigma_{\rm app} \propto \int \frac{F(E_{\rm cm})}{\sqrt{E_{\rm cm}E_{\rm d}}}{\rm d}E_{\rm cm}. \quad (15)$$

The corresponding curves for C^+, N^+ and O^+ are scaled to the data in Figures 2a–2c.

5 Presentation and discussion of the experimental results

Figures 2a–2c display our measured associative ionisation cross-section curves as a function of the centre-of-mass energy of the ionic reactants. The critical issue connected to the energy resolution of the apparatus is discussed above and is such that we restricted our presentation to energies greater than 10 meV. The error bars along the vertical axis represent only the statistical uncertainties on the cross-sections. The graphs do not include the 6% systematic uncertainties that we estimate to be at a one sigma level, in order to show the overall shape of the measured cross-sections. The systematic uncertainties are divided as follows: 3% on the interaction length, 1% on both beam intensities, 1% on the relative velocity and 5% on the scanning area $S_>$, every contribution being added quadratically. At 10 meV, the cross-sections are in the 10^{-14} cm^2 range, thus ten times greater than those found for $He^+ + H(D)^- \rightarrow HeH(D)^+ + e$ [12] or $H_2(D_2)^+ + H(D)^- \rightarrow H_3^+(H_2D^+, HD_2^+$ or $D_3^+) + e$ [13]. We shall first describe each studied system individually and then make a comparison.

The associative ionisation (AI) process is presented in Figure 2a. The full line below 1 eV represents the effective cross-section obtained by folding the calculated collision energy distribution with a model cross-section with a E^{-1} energy dependence, typical of a pure Coulomb interaction (see section above). The model fits extremely well our data and especially the apparent departure from this energy dependence below 40 meV and due to the finite energy resolution of our apparatus. At very low centre-of mass energy, the AI process populates few electronic states of the molecular cation CO^+ and for each of them, several ro-vibrational levels. Therefore, this measurement refers to total AI cross-sections. The electronic states are: $X^2\Sigma^+$, $A^2\Pi$, $B^2\Sigma^+$ (the two first ones correlate to $C^+(^2P) + O(^3P)$ and the latter one to $C^+(^2P) + O(^1D)$) and are shown in Figure 3a that displays the potential curves relevant to this study. At higher energies, the contributions of the states $C^2\Delta_r$ (not shown in the figure) and $D^2\Pi$ (that correlates to $C^+(^2P) + O(^3P)$) might be large as well. If one assumes that the associative flux is one hundred percents efficient to populate one of the specific

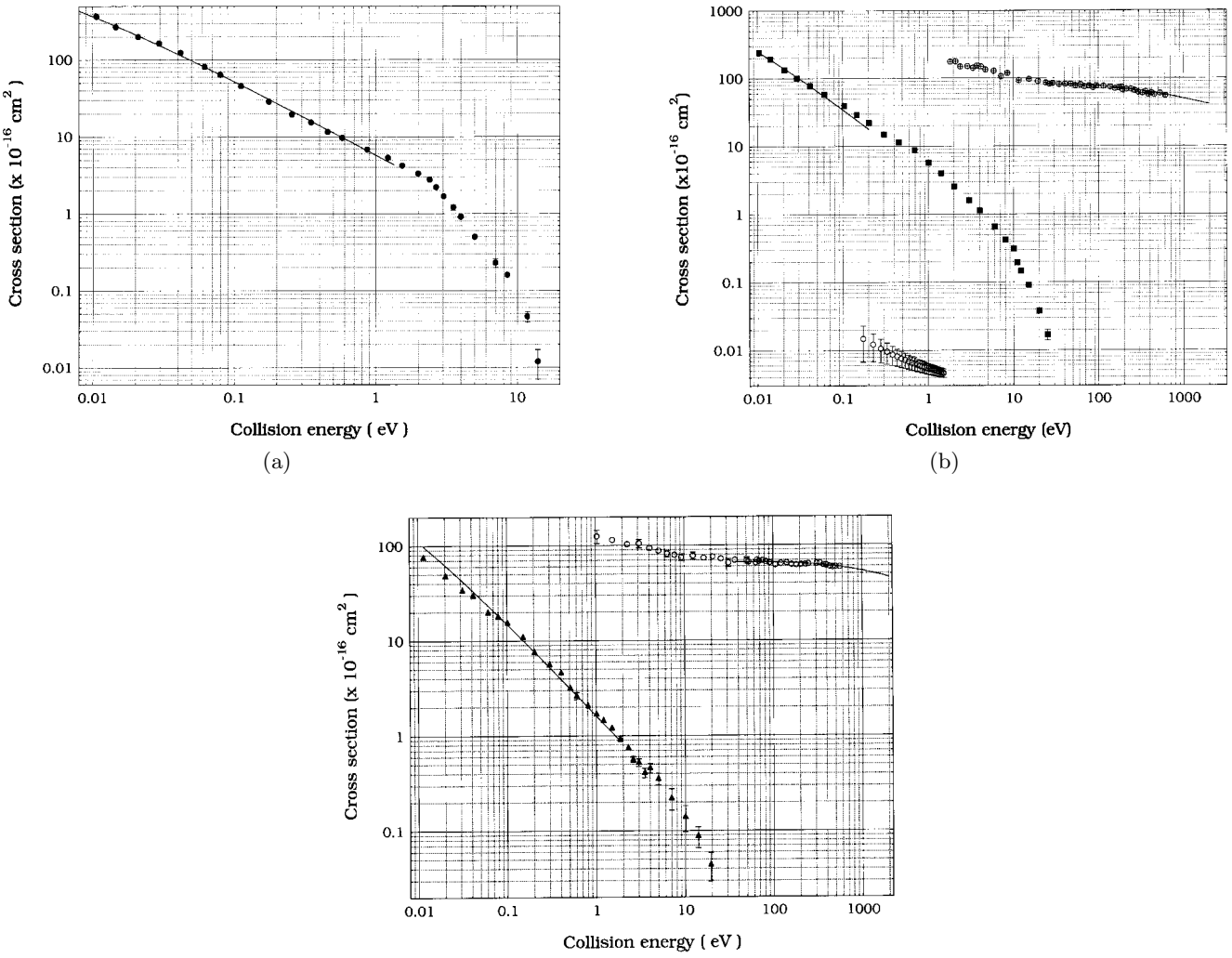

Fig. 2. Total AI cross-sections. (a) The data in full circles represent the associative ionisation process for $C^+ + O^-$ whereas the full line shows the normalised data with the E^{-1} dependence (see text). (b) The data in full squares represent the associative ionisation process for $N^+ + O^-$ whereas the full line on the AI curve shows the normalised data with the E^{-1} dependence (see text). The data in open circles are those concerning the AI process for the $NO^+(X^1\Sigma^+, v = 0)$ channel obtained by Le Padellec *et al.* [25] and using the DB model. The data in open circles with a cross, represent the mutual neutralisation cross-sections by Hayton and Peart [29] with a high energy extension in full line, also by the same authors. (c) The data in full triangles represent the associative ionisation process for $O^+ + O^-$ whereas the full line shows the normalised data with the E^{-1} dependence (see text). The data in open circles represent the mutual neutralisation cross-sections by Hayton and Peart [29] with the same type of high energy extension than in (b), in full line.

electronic states mentioned just above, an upper limit to the AI cross-section is:

$$\sigma_{\mathrm{AI}}(E_{\mathrm{cm}}) = \frac{\pi(N_{\max}+1)^2\hbar^2}{2\mu E_{\mathrm{cm}}} \cdot \qquad (16)$$

The energy dependent $N_{\max}$ is related to the centrifugal distortion of the potential curve corresponding to this electronic state, the reduced mass of the interacting system is μ and the AI centre-of-mass energy is E_{cm}. The suitable $N_{\max}$ for the $X^2\Sigma^+$ ground state at 10 meV collision energy is around 180, which gives a cross-section of 3.0×10^{-13} cm^2. The measured value is 3.7×10^{-14} cm^2, thus eight times lower than the former value, and is therefore an indication that electronically excited states of the molecular cation CO^+ might be populated by the AI process (the corresponding $N_{\max}$ for these states are smaller). It could also arise from the low multiplicity of the reaction channel responsible for AI.

It is very difficult (if not impossible) to give a qualitative and quantitative description of this AI process due to the poverty of the relevant molecular data. Indeed, we know from the correlation rules that twelve states correlate to the $C^+(^2P) + O^-(^2P)$ limit and seven of them, poorly known if at all, are shown in Figure 3a. These are

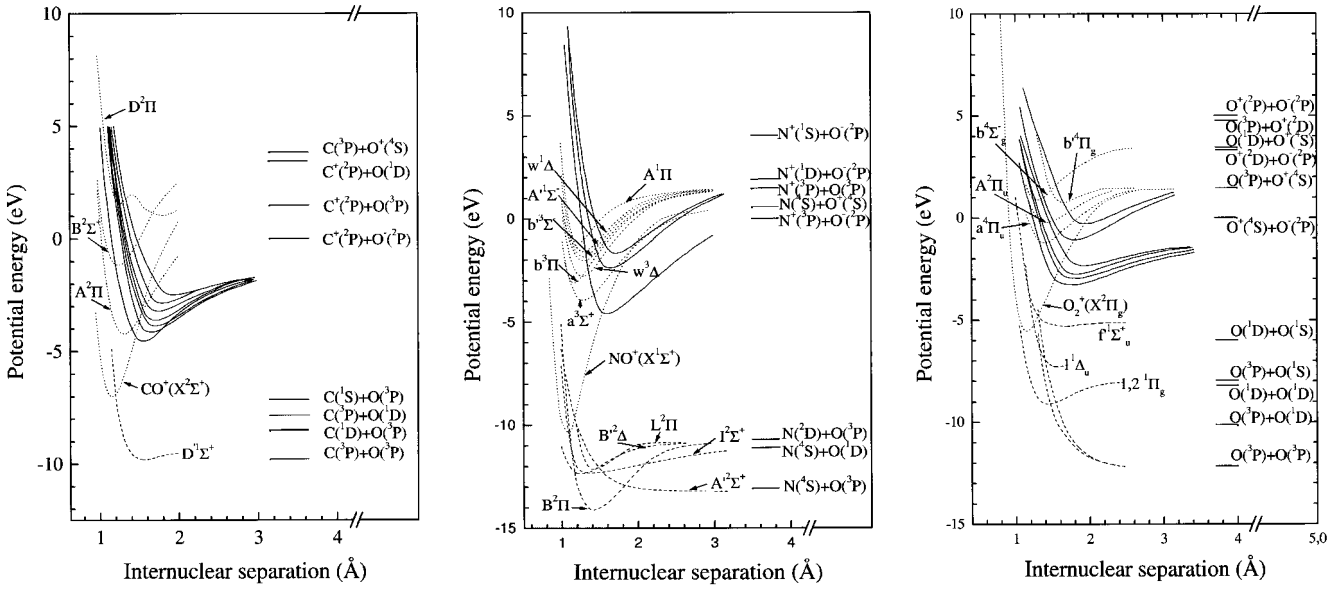

Fig. 3. Potential curves relevant to this study. The conventions are the following. The full lines represent the neutral states with the ion pairs as asymptotic limits, taken from [32]. The dotted lines represent the ionic states whereas the dashed ones are those for the neutral states with the neutral asymptotic limits. (a) Potential curves relevant to the $C^+ + O^-$ system. (b) Potential curves relevant to the $N^+ + O^-$ system. (c) Potential curves relevant to the $O^+ + O^-$ system.

the $^{1,3}\Sigma^+(2)$, $^{1,3}\Sigma^-(1)$, $^{1,3}\Pi(2)$ and $^{1,3}\Delta(1)$ states. The numbers in parentheses represent the number of electronic states of that particular symmetry. As can be seen in the figure, the crossings between these neutral curves (that correlate to the $C^+(^2P) + O^-(^2P)$ asymptote) and the cationic curves appear more favourable for the production of the CO^+ ($A^2\Pi$ and $B^2\Sigma^+$, low v) states than for the CO^+ ($X^2\Sigma^+$) ground state. This is in concord with the point made above. Depending upon what is the center-of-mass energy of the $C^+ + O^-$ system, several channels are (or become) open over the studied energy range (<20 eV):

$$\rightarrow CO(X^1\Sigma^+)+20.89 \text{ eV} \quad (17a)$$

$$\rightarrow C(^3P)+O(^3P)+9.80 \text{ eV} \quad (17b)$$

$$\rightarrow CO^+(X^2\Sigma^+)+e+6.88 \text{ eV} \quad (17c)$$

$$C^+(^2P)+O^-(^2P) \rightarrow C^+(^2P)+O(^3P)+e-1.46 \text{ eV} \quad (17d)$$

$$\rightarrow C^-(^4S)+O^+(^4S)-2.56 \text{ eV} \quad (17e)$$

$$\rightarrow C(^3P)+O^+(^4S)+e-3.82 \text{ eV} \quad (17f)$$

$$\rightarrow C^+(^2P)+O^+(^4S)+2e-15.08 \text{ eV} \quad (17g)$$

$$\rightarrow CO^{2+}(X^3\Pi)+2e-20.38 \text{ eV}. \quad (17h)$$

The three first channels are always open. In the mid seventies, Locht [24] reported an experimental work concerning the radiative association (Eq. (17a)). To the best of our knowledge, nothing has ever been reported on the mutual neutralisation (MN) process of $C^+ + O^-$ (Eq. (17b)), contrary to the $N^+ + O^-$ and $O^+ + O^-$ systems, see below. The neutral dissociative states of CO are responsible for this process but are unfortunately poorly known; one of them, the $D'^1\Sigma^+$, is represented in Figure 3a and correlates to the ground state $C(^3P) + O(^3P)$ limit. Moreover, this might not be the most contributing state since the MN process is essentially a large impact parameter process (see the $N^+ + O^-$ section). The associative ionisation (Eq. (17c)), together with the other five processes, has never been the subject of any reported work prior to this one. There is an interplay between the six ionisation processes (Eqs. (17c–17h)), and also those occurring at even higher energies, where the measured cross-section is vanishingly small. For the description of the channel interplay, one shall refer to Figure 4 where the curve σE is plotted against E (in full circles), a useful representation to amplify curve fluctuations. Below about 1 eV, and apart from the points below 40 meV affected by the energy resolution (see above), only a structureless E^{-1} energy dependence can be seen, which obviously gives a constant σE in the representation we have chosen. Between 1 and 3 eV, a rather weak positive signal on top of this E^{-1} dependence is observed, due to the increasing number of accessible rovibrational levels in CO^+. This might obliterate the competition with the $C^+(^2P) + O(^3P) + e$ channel, expected to reduce the AI probability above 1.46 eV. On the other hand, the rapid fall-off of our measured cross-sections above 2.4 eV does not coincide with the opening of the $C(^3P) + O^+(^4S) + e$ channel. One is left with the $C^-(^4S) + O^+(^4S)$ and $C^+(^2P) + O(^3P) + e$ channels

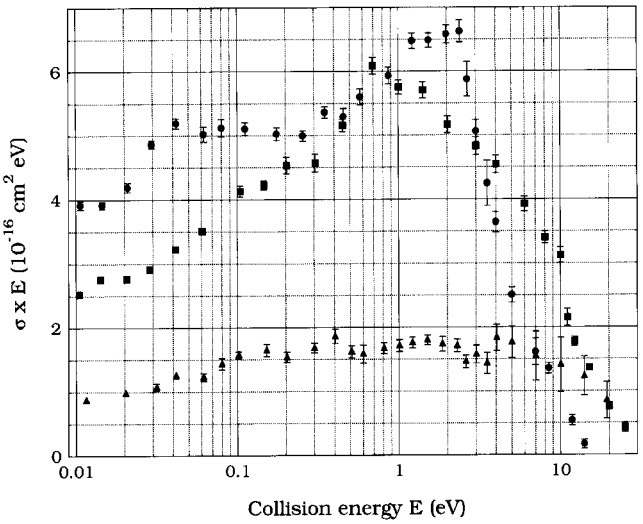

Fig. 4. σE over E representation (see text). Same symbol conventions as in Figure 2.

to explain the sudden drop of the cross-section. The slow predissociation of highly excited rotational states of CO^+ may add to the molecular ion yield recorded in the experiment, and hence delay the fall-off of the cross-section to energies above the centrifugal barrier, the magnitude of which we estimate to be around 0.6 eV. The cross-sections become weaker and weaker to reach a non-measurable level just below 15 eV where they present an even more abrupt decrease. This might be connected to the opening of the $C^+(^2P) + O^+(^4S) + 2e$ channel to which the $CO^{2+}(X^3\Pi)$ correlates.

The corresponding AI process is displayed in Figure 2b. The full line below 1 eV represents the effective cross-section for a pure E^{-1} dependence, as explained above. The model fits reasonably well the data below 0.2 eV. At very low centre-of-mass energy, few electronic states of the NO^+ ions can be populated and for each of them, several ro-vibrational levels. These electronic states, displayed in Figure 3b, are: $X^1\Sigma^+$, $a^3\Sigma^+$, $b^3\Pi_p$, $w^3\Delta$, $b'^3\Sigma^-$, $A'^1\Sigma^-$, $w^1\Delta$ and $A^1\Pi$ (the two first ones correlate to $N(^4S) + O^+(^4S)$ and the latter ones to $N^+(^3P) + O(^3P)$). Using again equation (16) with the suitable energy dependent $N_{\max}$ for $NO^+(X^1\Sigma^+)$, that is to say about 220, one gets a value slightly larger than what was found for CO^+ for the cross-section at 10 meV, thus 4.3×10^{-13} cm^2. The measured value is around 2.4×10^{-14} cm^2, thus about eighteen times lower than the former value, and might indicate that electronically excited states of NO^+ are populated by the AI process. We know from the correlation rules that twelve states correlate to the lowest $N^+(^3P) + O^-(^2P)$ limit and one of them is shown in Figure 3b. The contribution to AI of a small fraction of those entrance channels can explain the lower value observed for the cross-section. These are the $^{2,4}\Sigma^+(1)$, $^{2,4}\Sigma^-(2)$, $^{2,4}\Pi(2)$, and $^{2,4}\Delta(1)$ states. For the next limit, $N^+(^1D) + O^-(^2P)$, there are nine ($^2\Sigma^+(2)$, $^2\Sigma^-(1)$, $^2\Pi(3)$, $^2\Delta(2)$, $^2\Phi(1)$) correlating states and two of them are displayed in Figure 3b. The crossings between the neutral potential curve that correlates to $N^+(^3P) + O^-(^2P)$ and the cationic potential curves, seem to favour the production of NO^+ excited states with low vibrational quanta, while for the ground state $NO^+(X^1\Sigma^+)$, this crossing occurs at large v. The point made concerning the disfavoured contribution of the $X^1\Sigma^+$ ground state ($v = 0$) ion is in perfect agreement with the recent finding by Le Padellec *et al.* [25]. Indeed, using the heavy ion storage ring CRYRING located at Stockholm University, they measured the ion pair formation from the dissociative recombination of $NO^+(X^1\Sigma^+, v = 0)$, namely the reverse process to that under study. They made use of a simple model based on the detailed balance principle and extracted the useful information that the $NO^+(X^1\Sigma^+, v = 0)$ channel is a very minor product of the AI process; the extrapolated data are shown in Figure 2b. Depending upon what is the center-of-mass energy of the $N^+ + O^-$ system, several channels are (or become) open over the studied energy range (<30 eV):

$$\rightarrow NO(X^2\Pi_r)+19.55 \text{ eV} \quad (18a)$$

$$\rightarrow N(^4S)+O(^3P)+13.07 \text{ eV} \quad (18b)$$

$$\rightarrow NO^+(X^1\Sigma_r^+)+e+10.29 \text{ eV} \quad (18c)$$

$$N^+(^3P)+O^-(^2P) \rightarrow N(^4S)+O^+(^4S)+e-0.54 \text{ eV} \quad (18d)$$

$$\rightarrow N^+(^3P)+O(^3P)+e-1.46 \text{ eV} \quad (18e)$$

$$\rightarrow N^+(^3P)+O^+(^4S)+2e-15.07 \text{ eV} \quad (18f)$$

$$\rightarrow NO^{2+}(X^2\Sigma_r^+)+e-18.85 \text{ eV}. \quad (18g)$$

The three first channels are always open. To the best of our knowledge, nobody has ever reported on the radiative association in $N^+ + O^-$ collisions (Eq. (18a)). Nevertheless, the comments made concerning the previous system are still valid. At least four works were reported on the mutual neutralisation of $N^+ + O^-$ (process (18b)): by Aberth and Peterson [26], Olson *et al.* [27], Peart *et al.* [28] and Hayton and Peart [29]. The two former works give results that differ from the two latter ones, but according to Peart *et al.*, it might be possible to rationalise these discrepancies by the difference in internal excitation of the N^+ target. The issue connected with the possible presence of metastable states in the cationic beams is indeed a critical one. We decided to display in Figure 2b the results from the most recent work by Hayton and Peart [29] in order to show how they compare with our AI data. If the entrance channel is the same ($N^+ + O^-$), there are some important differences. Indeed, the mutual neutralisation is essentially a "long-range" process whereas the associative ionisation is typically taking place at shorter internuclear distances, in the Franck-Condon region. If one extrapolates Hayton and Peart's data at lower energy with a E^{-1} dependence, one gets a value of 3.2×10^{-12} cm^2 at 10 meV, and therefore an averaged impact parameter of $\sqrt{\sigma/\pi} = 101$ Å.

To some extent, some of the neutral dissociative states of NO that are mainly relevant to the dissociative recombination process, might also contribute to the MN process. The corresponding potential energy curves of NO ($B^2\Pi$, $A'^2\Sigma^+$, $I^2\Sigma^+$, $B'^2\Delta$ and $L^2\Pi$) are shown for

completeness. The associative ionisation (Eq. (18c)) is the main subject of the present paper and, together with the other four processes (Eqs. (18d–18g)), has never been the subject of any reported work prior to this one. There is again interplay between these five ionisation processes (Eqs. (18c–18g)) and we again make use of the σE representation in Figure 4. Below about 0.4 eV and apart from the points below 100 meV affected by the energy resolution (see above), only a structureless E^{-1} energy dependence can be seen in Figure 2b and to less extent in Figure 4. Between 0.4 and 2 eV, a rather weak positive signal on top of the E^{-1} dependence is observed in Figure 4, due to newly accessible ro-vibrational levels of NO^+, which might obliterate the opening of the $N(^4S) + O^+(^4S) + e$ channel at 0.54 eV. The faster decrease of the cross-section, occurring above 0.9 eV, may be produced by that channel, when no more long-lived rotational states of NO^+ can be formed that would survive the time of flight to the detector, namely above the 0.6 eV centrifugal barrier. However, its effect seems to be much weaker than in the CO^+ case. The population of that dissociative channel requires a major rearrangement of the system, and corresponds to transfer ionisation, instead of a simple electron detachment for $C^+ + O^-$ collisions. The rapid fall-off observed above 10 eV does not seem to coincide with the opening of the $N^+(^3P) + O(^3P) + e$ channel, which occurs at 1.46 eV according to the energetics. At larger energies, the cross-sections become weaker and weaker to reach a non-measurable level just below 20 eV. This might have something to do with the opening of the $N^+(^3P) + O^+(^4S)+2e$ channel to which the $NO^{2+}(X^2\Sigma^+)$ correlates.

The AI process originating from $O^+ + O^-$ is presented in Figure 2c. The full line below 1 eV represents the convolution of a model cross-section scaled to our data. At very low centre-of-mass energy, few electronic states of the O_2^+ ions can be populated and for each of them, several ro-vibrational levels. These electronic states are: $X^2\Pi$, $a^4\Pi_u$ and $A^2\Pi_u$, all correlating to $O(^3P) + O^+(^4S)$. At larger energies, the excited states $b'^4\Pi_g$, $b^4\Sigma_g^-$ and $C^2\Phi_u$ might be populated as well, the two former ones correlating to $O(^1D) + O^+(^4S)$ and the latter one to $O(^3P) + O^+(^2P)$. Exception made of the $C^2\Phi_u$ state, all the corresponding potential curves are displayed in Figure 3c. Again, one can make use of expression (16) together with the suitable $N_{\max}$ value of 175 for the O_2^+ ground state. For the AI cross-section at 10 meV, this would give a value of 2.55×10^{-13} cm^2 that shall be compared to our about thirty times lower value of 0.8×10^{-14} cm^2, and is again a good indication that excited states of O_2^+ are populated, although multiplicities of the entrance channels may as well be responsible for the low AI cross-section. We know from the correlation rules that eight states correlate to the lowest $O^+(^4S) + O^-(^2P)$ limit and four of them are displayed in Figure 3c. These are the $^{3,5}\Sigma_{u,g}^+(1)$ and $^{3,5}\Pi_{u,g}(1)$ states. For the next limit, $O^+(^2D) + O^-(^2P)$, among the thirty-six correlating states, $^{3,5}\Sigma_{u,g}^+(2)$, $^{3,5}\Sigma_{u,g}^-(1)$, $^{3,5}\Pi_{u,g}(3)$, $^{3,5}\Delta_{u,g}(2)$ and $^{3,5}\Phi_{u,g}(1)$, two of them are also shown in Figure 3c. Depending upon what is the center-of-mass energy of the $O^+ + O^-$ system, several channels are (or can be open) over the studied energy range (<20 eV):

$$\rightarrow O_2(X^3\Sigma_g^-)+17.27 \text{ eV} \quad (19a)$$

$$\rightarrow O(^3P)+O(^3P)+12.15 \text{ eV} \quad (19b)$$

$$O^+(^4S)+O^-(^2P) \rightarrow O_2^+(X^2\Pi_g)+e+5.20 \text{ eV} \quad (19c)$$

$$\rightarrow O(^3P)+O^+(^4S)+e-1.46 \text{ eV} \quad (19d)$$

$$\rightarrow O^+(^4S)+O^+(^4S)+2e-15.07 \text{ eV} \quad (19e)$$

$$\rightarrow O_2^{2+}(X^1\Sigma_g^+)+2e-18.65 \text{ eV}. \quad (19f)$$

The three first processes are always open. Lacome [30] has reported on the (radiative) association in $O^+ + O^-$ collisions (process (19a)) whereas Martin and Hepburn [31] performed a study of the energetic thresholds for the ion-pair photodissociation of diatomic oxygen, namely the reverse process to the previous one. They selectively highlighted the presence (importance) of highly vibrationally excited ion-pair states that are not relevant to our study since these are extremely long-lived (in the microsecond range), and therefore unlikely to be populated by inverse predissociation. Moreover, three works were performed on the mutual neutralisation of $O^+ + O^-$ (process (19b)): by Olson *et al.* [27], Peart *et al.* [28] and Hayton and Peart [29], and the results by the latter contributors are displayed in Figure 2c. Extrapolating their data at low energy with a E^{-1} dependence, one gets a value of 1.3×10^{-12} cm^2 at 10 meV, and therefore an averaged impact parameter of 64 Å.

In this framework, few O_2 dissociative states, the $1, 2\,^1\Pi_g$, $1\,^1\Delta_u$ and $f''\,^1\Sigma_u^+$ curves are shown for completeness. There is interplay between the four processes (19c–19f). Indeed below about 7 eV, only a structureless E^{-1} energy dependence can be seen with the σE representation in Figure 4. The opening of the $O(^3P) + O^+(^4S) + e$ channel that shall occur at 1.46 eV, does not give rise to any special accident in the cross-section curve. The shallow fall-off above 10 eV might have something to do with the opening of the $O^+(^4S) + O^+(^4S)+2e$ channel, to which the $O_2^{2+}(X^1\Sigma_g^+)$ correlates.

Figure 4 displays the three AI cross-section curves (C^+, N^+, $O^+ + O^-$) for comparison, in the $\sigma \times E$ representation. At 10 meV, the theoretical prediction by equation (16) is not reproduced experimentally, that is to say that the AI process is observed to decrease in efficiency from $C^+ + O^-$ to $N^+ + O^-$ and again to $O^+ + O^-$; the "experimental" ratios $\sigma(C^+ + O^-)/\sigma(N^+ + O^-)$ and $\sigma(C^+ + O^-)/\sigma(O^+ + O^-)$ are 1.52 and 4.72, respectively. This can be rationalised since equation (16) refers to one particular electronic state and we have shown above in the section describing the individual results, that the AI process populates several states, and arises from the autoionisation of one or more specific channels of unknown statistical weight. Below 2 eV, the $C^+ + O^-$ and $N^+ + O^-$ AI curves are fairly identical in shape and magnitude, and it is only above 2.4 eV that a more rapid fall-off is observed for the $C^+ + O^-$ channel. By plotting the

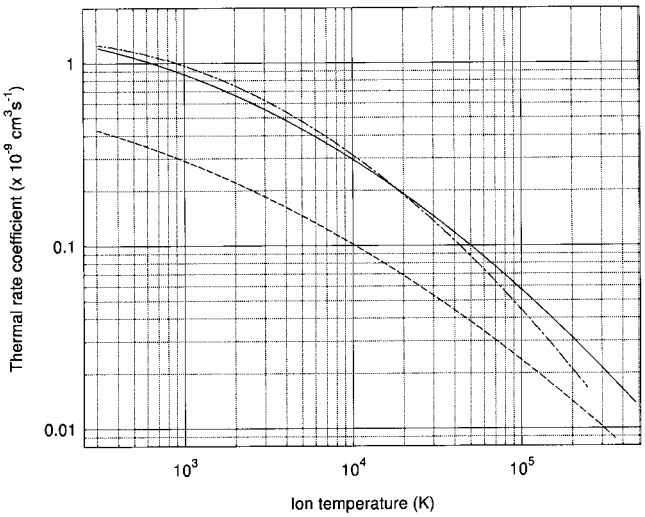

Fig. 5. Inter-comparison of the AI thermal rate coefficients *versus* ionic temperature. The line conventions are the following: dashed-dotted line for the $C^+ + O^-$ system, full line for the $N^+ + O^-$ system and dashed line for the $O^+ + O^-$ system.

product of the cross-sections by the centre-of-mass energy in Figure 4, one reveals the sudden fall-off discussed in the former paragraphs. One clearly sees the rise of the cross-section as more and more ro-vibrational levels are populated in the molecular cation, and the abrupt decrease at an energy substantially larger than the expected thresholds (presence of a centrifugal barrier). The $O^+ + O^-$ AI curve exhibits a similar shape than the former ones, but a much lower magnitude.

Figure 5 displays the associative ionisation thermal rate coefficients (expressed in $cm^3\,s^{-1}$) as a function of the ionic temperature (expressed in K) for the three systems under study. The general features mentioned above in the intercomparison of the cross-section curves are still visible. These coefficients, useful for plasma studies and derived from the following relation:

$$\alpha(T) = \frac{8\pi\mu}{(2\pi\mu k_B T)^{3/2}} \int_0^\infty \sigma(E_{cm}) E_{cm} \times \exp(-E_{cm}/k_B T) \mathrm{d}E_{cm} \quad (20)$$

with μ the reduced mass of the system $X^+ + O^-$, are most relevant when the ionic temperature is lower than 17 000 K, which is equivalent to the 1.46 eV electron affinity of the oxygen atom.

6 Conclusion

The cross-sections for the associative ionisation process in (C^+, N^+ and O^+) + O^- collisions were measured using a merged beam set-up. We have shown that this process might be relevant to plasma studies and therefore, we also presented the thermal rate coefficients after the results were discussed. The experimental set-up had been slightly modified since previous studies, and the changes were stressed in a devoted paragraph. Special attention was drawn of the internal energy of the target cation as any excitation could affect the cross-section measurements. Unfortunately, if we were able to prove their presence in our cationic beams, we were not successful with the quantification of their contributions. Since we achieved, by assuming ground state ionic reactants, the clear assignments of most of the features that appear in our different AI spectra, this could mean that we mainly dealt with internally cold reactants. The issue connected to the energy resolution was also addressed and from that respect, we are confident with the reliability of our results, especially at low energy. Our data were presented next and put in perspective with results concerning other competing processes to the associative ionisation, if these would be available in the literature. In fact, most of the existing data concern the "longer range" mutual neutralisation process. Our most important result concerns the large size of the measured cross-sections as these reach values in the 1×10^{-14} cm^2 range at thermal energies. We made an attempt to discuss our data in a qualitative way, but this was limited due to the very lack of (reliable) molecular data. In that respect, this is our hope that future work would be carried out on that subject (as well as on related topics), both experimentally and theoretically.

This work was funded by the Belgian National Fund for Scientific Research (FNRS) and the Euratom-Belgian state association. One of us (ALP) would like to acknowledge this financial support that made possible his six months visit at the "Université Catholique de Louvain".

References

1. P. Bouchet, E. Slezak, T. LeBertre, A. Moneti, J. Manfroid, Astron. Astroph. **80**, 379 (1989).
2. A. Dalgarno, M.L. Du, J.H. You, Astroph. J. **349**, 675 (1990).
3. A. Dalgarno, *Dissociative Recombination: theory, experiment and applications*, edited by B.R. Rowe, J.B.A. Mitchell, A. Canosa (Plenum Press, New York, 1993), p. 243.
4. M. Mandelman, T. Carrington, R.A. Young, J. Chem. Phys. **58**, 84 (1973).
5. S.E. Nielsen, J.S. Dahler, J. Chem. Phys. **71**, 1910 (1979).
6. G. Ringer, W.R. Gentry, J. Chem. Phys. **71**, 1902 (1979).
7. C. Bertrand, P.J. van Tiggelen, J. Phys. Chem. **78**, 2320 (1974).
8. M.A. Bredo, P.J. Guillaume, P.J. van Tiggelen, *Fifteenth symposium on Combustion* (Tokyo, Japan, 1974), p. 1003.
9. J.F. Babb, A. Dalgarno, Phys. Rev. A **51**, 3021 (1995).
10. M. Capitelli, E. Ficocelli, J. Phys. B **5**, 2066 (1972).
11. K. Olamba, S. Szucs, J.P. Chenu, E.A. Naji, F. Brouillard, J. Phys. B **29**, 2837 (1996).
12. E.A. Naji, K. Olamba, J.P. Chenu, S. Szucs, M. Chibisov, F. Brouillard, J. Phys. B **31**, 2961 (1998).
13. E.A. Naji, K. Olamba, J.P. Chenu, S. Szucs, F. Brouillard, J. Phys. B **31**, 4887 (1998).

14. K. Olamba, S. Szücs, J.P. Chenu, A. Naji, F. Brouillard, *Twentieth International Conference on the Physics of Electronic and Atomic Collisions*, Book of Abstracts FR 200, edited by F. Aumayr, G. Betz, H.P. Winter, Vienna, Austria, 1997.
15. C. Moore, NSRDS-NBS 35, Washington DC, 1971.
16. J.M. Ajello, J. Chem. Phys. **55**, 3158 (1971).
17. J. Berkowitz, J.H.D. Eland, J. Chem. Phys. **67**, 2740 (1977).
18. A.P. Hitchcock, C.E. Brion, M.J. van der Wiel, Chem. Phys. **45**, 461 (1980).
19. M. Hamdan, A.G. Brenton, J. Phys. B **22**, 2289 (1989).
20. C.J. Reid, J. Phys. B **25**, 475 (1992).
21. M.F.A. Harrison, K. Dolder, P.C. Thonemann, Proc. Phys. Soc. **82**, 368 (1963).
22. C.R. Blakley, M.R. Vestal, J.H. Futrell, J. Chem. Phys. **66**, 2392 (1977).
23. C. Sheehan, A. Le Padellec, W.N. Lennard, D. Talbi, J.B.A. Mitchell, J. Phys. B **32**, 3347 (1999).
24. R. Locht, Chem. Phys. Lett. **34**, 508 (1975).
25. A. Le Padellec, N. Djurić, A. Al-Khalili, H. Danared, A.M. Derkatch, A. Neau, D.B. Popović, S. Rosén, J. Semaniak, R. Thomas, M. af Ugglas, W. Zong, M. Larsson, Phys. Rev. A **64**, 012702 (2001).
26. W.H. Aberth, J.R. Peterson, Phys. Rev. **1**, 158 (1970).
27. R.E. Olson, J.R. Peterson, J. Moseley, J. Chem. Phys. **53**, 3391 (1970).
28. B. Peart, S.J. Foster, K. Dolder, J. Phys. B **22**, 1035 (1989).
29. D.A. Hayton, B. Peart, J. Phys. B **26**, 2879 (1993).
30. N. Lacome, thèse de doctorat, France, 1994.
31. J.D.D. Martin, J.W. Hepburn, Phys. Rev. Lett. **79**, 3154 (1997).
32. R. Locht, J. Momigny, Int. J. Mass Spectrom. Ion Phys. **7**, 121 (1971).